Quantum Electronics **51** (9) 850–853 (2021)

https://doi.org/10.1070/QEL17619

Generation of IR radiation in the interaction of an ultrashort laser pulse with a gas jet

A.A. Golovanov, I.Yu. Kostyukov

Abstract. **We consider the generation of IR radiation during the interaction of a high-power ultrashort laser pulse with a gas jet using numerical simulation by the particle-in-cell method. The laser pulse parameters correspond to the capabilities of the PEARL sub-petawatt laser facility in Nizhny Novgorod (Russia) when using the compression after compressor approach (CafCA). It is demonstrated that about 1 % of the energy can be converted into radiation in the wavelength range of 5–10 μm.**

Keywords: *IR radiation, wake wave, strongly nonlinear regime, particle-in-cell method.*

1. Introduction

Sources of high-power short pulses in the IR range are in demand in many fields of application. Significant progress has been made in generating pulses in the mid-IR range (with a wavelength of up to 5 μm); however, in the far-IR range (more than 5 μm), pulse generation causes difficulties due to the lack of optical materials with a suitable wide gain band and a rather high radiation resistance.

As one of the possible methods for generating radiation in the far-IR range, it was proposed to use the interaction of a high-power laser pulse with a rarefied plasma [1, 2]. The generation of IR radiation in this case occurs due to the effect of photon deceleration on the plasma density gradient that arises in a wake wave excited by a laser pulse [3]. Generation by this mechanism has been demonstrated in experiments [1, 4].

Significant results in the generation of high-power short (single-period) IR pulses with an adjustable frequency have been achieved by using specially created plasma profiles [4, 5]. The process of interaction with plasma consisted of three stages: laser pulse compression in a plasma with a lower density, generation of radiation in the IR range in a plasma with a higher density, and radiation extraction.

An alternative to the plasma compressor stage may be other methods of obtaining ultrashort sub-petawatt pulses, in particular, the compression after compressor approach (CafCA). This approach consists in additional temporal pulse compression after the compressor, used in the chirped pulse amplification technique [6], due to the use of nonlinear plates with a large aperture [7, 8]. This method is successfully used to compress high-power short laser pulses (with a duration of several tens of femtoseconds and an energy of more than 10 J), including in experiments at the PEARL facility [9] at the Institute of Applied Physics of the Russian Academy of Sciences (Nizhny Novgorod, Russia) [10, 11]. In particular, the PEARL facility demonstrated threefold compression (from 63 to 21 fs) of a laser pulse with an energy of 12 J with an efficiency of almost 100 % [10].

In this work, the generation of radiation in the IR range during the interaction of a high-power ultrashort laser pulse with a gas jet is studied using numerical simulation by the particle-in-cell (PIC) method [12, 13].

2. Interaction simulation

To study the IR pulse generation, a three-dimensional numerical simulation of the interaction of a laser pulse with plasma was carried out using the particle-in-cell method. The pulse parameters corresponded to the capabilities of the PEARL sub-petawatt laser facility when compressing the generated pulse with a duration of about 50–60 fs by the CafCA method. In the simulation, the initial duration of the linearly polarised pulse was 19 fs (FWHM in intensity), the spot size was 16 μm (half-width at intensity level $1/e^2$) at $f/20$ focusing, and the energy was 10 J, which corresponded to a peak power of about 500 TW. The laser radiation wavelength was λ_L = 910 nm. The pulse interacted with a plasma having a maximum electron density of 10^{19} cm^{-3} and a trapezoidal longitudinal profile, which provided a smooth increase and decrease in the plasma density and consisted of a 0.2 mm long section of linear increase in density from zero to the maximum value, a horizontal plateau with a length of 0.6 mm, and a 0.2 mm long section of linear decay in density to zero. Such a plasma profile models the interaction of a laser pulse with a thin supersonic gas jet.

The Quill software package [14] based on the particle-in-cell method was used for simulation. The size of the simulation domain was $60\lambda_L \times 80\lambda_L \times 80\lambda_L$ with spatial steps of $0.05\lambda_L$ and $0.15\lambda_L$ in the longitudinal (x, along the direction of the laser pulse propagation) and two transverse (y and z) directions, respectively. The laser radiation was polarised along the y axis. The initial number of particles in the cell was equal to unity. The simulation relied on the NDFX (numerical-dispersion-free in the x direction) scheme to suppress the numerical dispersion in the direction of the laser pulse propa-

A.A. Golovanov, I.Yu. Kostyukov Institute of Applied Physics, Russian Academy of Sciences, ul. Ulyanova 46, 603950 Nizhny Novgorod, Russia; Lobachevsky State University of Nizhny Novgorod, prosp. Gagarina 23, 603950 Nizhny Novgorod, Russia; e-mail: agolovanov@ipfran.ru

Received 29 July 2021
Kvantovaya Elektronika **51** (9) 850–853 (2021)
Translated by M.A. Monastyrskiy

gation [15] and the adaptive moving window method to ensure moving of the simulation region at the laser pulse speed in plasma.

The laser pulse can be characterised by a dimensionless amplitude

$$a_0 = \frac{eE_{\max}}{mc\omega_L}, \tag{1}$$

where $E_{\max}$ is the maximum value of the electric field amplitude; ω_L is the laser field frequency; $e > 0$ is the elementary charge; m is the electron mass; and c is the speed of light. The value $a_0 \sim 1$ corresponds to the transition to the relativistic regime of interaction with plasma, when the plasma electrons oscillating in the laser field gain an energy comparable to the rest energy. The initial value of a_0 for the pulse under consideration was 8.9. Such a high-power laser pulse generates a strongly nonlinear wake wave in plasma (Fig. 1), which is characterised by the formation of a cavity free of plasma electrons behind the laser pulse. As the laser pulse propagates in plasma, plasma electrons are trapped into the plasma cavity as a result of the self-injection process [16], and their further acceleration occurs.

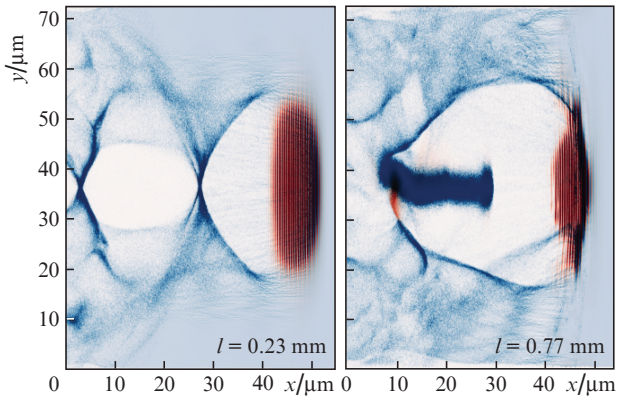

Figure 1. (Colour online) Distribution of electron density (blue colour) and laser intensity (red colour) in the cross section of the xy plane in the wake wave excited by a laser pulse for various pulse propagation lengths l in plasma. The laser pulse propagates along the x axis from left to right.

In the matched regime of strongly nonlinear interaction, when self-focusing and diffraction compensate for each other and the pulse propagates in the plasma without changing its transverse size, the laser beam spot size w_0 satisfies the condition [17]

$$k_p w_0 = 2\sqrt{a_0}, \tag{2}$$

where $k_p = \omega_p/c$ is the plasma wave number; $\omega_p = (4\pi e^2 \times n_p/m)^{1/2}$ is the electron plasma frequency; and n_p is the plasma density. This formula is valid for sufficiently short pulses (the longitudinal size of the pulse should not be much larger than the transverse one) with a relativistic intensity ($a_0 \gtrsim 2$). If we assume that the product $a_0 w_0 = I_0$ preserves its value (which corresponds to the conservation of the peak power proportional to $a_0^2 w_0^2$), then relation (2) will allow us to calculate the expected matched size depending on the initial laser pulse parameters and plasma density. The matched laser pulse spot size, which ensures stable pulse propagation, for the plasma density of 10^{19} cm^{-3} and the above parameters of the laser pulse, is 12 μm, which is slightly less than the initial size of 16 μm. Therefore, during propagation, the laser pulse was focused in the gas jet, as a result of which its amplitude increased (Fig. 2). In this case, the pulse duration was reduced by almost half.

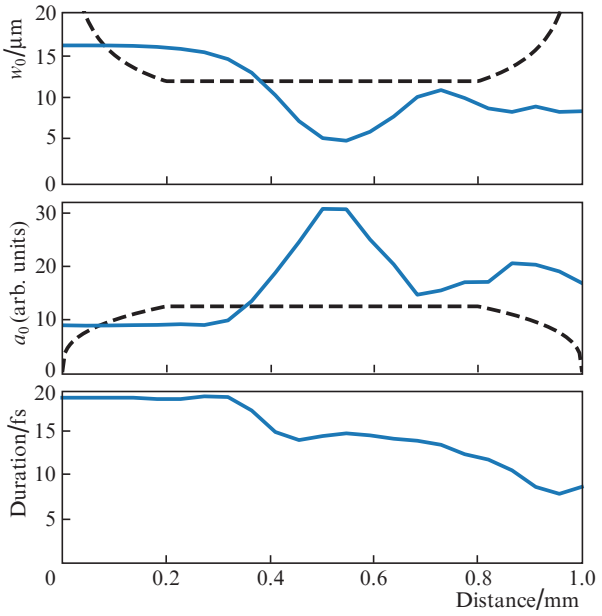

Figure 2. (Colour online) Evolution of the spot size w_0, the maximum dimensionless amplitude a_0, and the laser pulse duration depending on the distance travelled by the pulse. The dashed line shows the expected size and expected amplitude a_0 in a matched propagation regime for a given trapezoidal plasma profile, assuming that the product $a_0 w_0$ is preserved.

3. Spectral analysis

The field obtained as a result of simulation can be represented as a Fourier harmonic decomposition:

$$\boldsymbol{E}(\boldsymbol{r},t) = \int \tilde{\boldsymbol{E}}(\boldsymbol{k},t)\exp(\mathrm{i}\boldsymbol{k}\boldsymbol{r})\,\mathrm{d}^3\boldsymbol{k}, \tag{3}$$

$$\boldsymbol{B}(\boldsymbol{r},t) = \int \tilde{\boldsymbol{B}}(\boldsymbol{k},t)\exp(\mathrm{i}\boldsymbol{k}\boldsymbol{r})\,\mathrm{d}^3\boldsymbol{k}. \tag{4}$$

In this case, it is possible to represent the total energy of the electromagnetic field in space as

$$W = \int \frac{\boldsymbol{E}^2 + \boldsymbol{B}^2}{8\pi}\mathrm{d}^3\boldsymbol{r} = \pi^2 \int (|\tilde{\boldsymbol{E}}|^2 + |\tilde{\boldsymbol{B}}|^2)\mathrm{d}^3\boldsymbol{k}, \tag{5}$$

and thus, introduce the energy density distribution in wave vectors,

$$\frac{\mathrm{d}W}{\mathrm{d}\boldsymbol{k}} = \pi^2(|\tilde{\boldsymbol{E}}(\boldsymbol{k},t)|^2 + |\tilde{\boldsymbol{B}}(\boldsymbol{k},t)|^2). \tag{6}$$

It should be noted that the energy density introduced in this way does not allow distinguishing between the wave vectors $\boldsymbol{k}$ and $-\boldsymbol{k}$.

Assuming that the electromagnetic field obeys the vacuum dispersion relation $\omega = c|\boldsymbol{k}|$, we can formally introduce the spectral energy density

$$\frac{\mathrm{d}W}{\mathrm{d}\omega} = \frac{\pi^2}{c^3}\omega^2 \oint \left[\left| \tilde{\boldsymbol{E}}\left(\frac{\omega}{c}\boldsymbol{n}\right) \right|^2 + \left| \tilde{\boldsymbol{B}}\left(\frac{\omega}{c}\boldsymbol{n}\right) \right|^2 \right] \mathrm{d}^2\boldsymbol{n}, \qquad (7)$$

where $\boldsymbol{n} = \boldsymbol{k}/|\boldsymbol{k}|$, and the integration is performed over a sphere of unit radius. In fact, the assumption about the vacuum dispersion relation is generally incorrect, since at any time moment there is also a field of plasma currents $\boldsymbol{j}$ in space, and the fields $\boldsymbol{E}$ and $\boldsymbol{B}$ do not obey Maxwell's vacuum equations. In this case, we assume that their contribution to the spectral regions of interest is small.

Figure 3 shows the evolution of the electromagnetic field spectrum calculated by formula (7), depending on the distance travelled by the laser pulse. It can be seen that the spectrum is significantly broadened and shifted towards larger wavelengths. An additional local spectrum maximum is observed in the low-frequency region (wavelengths over 10 μm). As the component-wise spectral analysis shows (Fig. 4), this maximum largely contains the longitudinal electric field component E_x, as well as the transverse components of the fields E_z and B_y, which do not correspond to the initial pulse polarisation (along the y axis). This allows us to conclude that such a maximum corresponds to the contribution to the spectrum of the wake wave's electromagnetic field, as well as the Coulomb field of the accelerated electron bunch, which do not have a pronounced polarisation. These fields are not radiated electromagnetic waves, and so their contribution should be excluded from the calculation results. The effect of these fields is greatest for wavelengths exceeding 10 μm; therefore, to filter their contribution to long-wavelength IR radiation, it is assumed to use a limited wavelength range of 5–10 μm (the shaded region in Figs 3 and 4), in which the y polarised components E_y and B_z make a fundamental contribution to the overall spectral energy density (see Fig. 4). The isolation of the electromagnetic component in the wavelength range above 10 μm will require the use of more advanced analysis methods and is beyond the scope of this work.

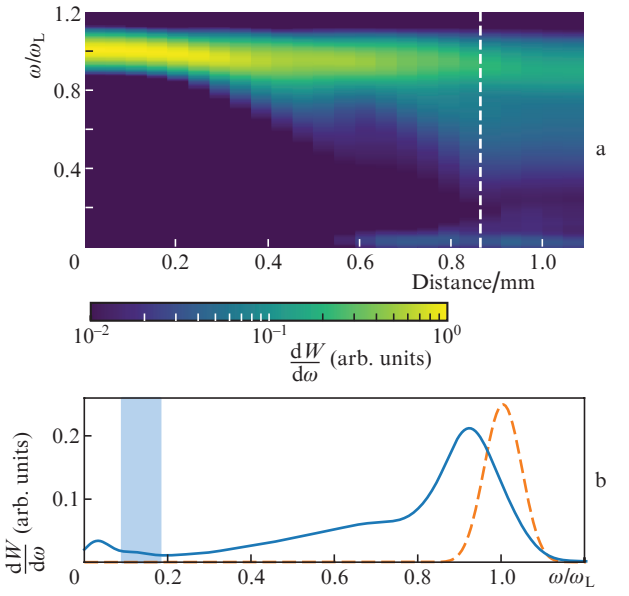

Figure 3. (Colour online) Evolution of the electromagnetic field spectrum during the propagation of a laser pulse in plasma (a) and the instantaneous spectrum (b, solid curve) for the distance shown by the vertical dashed line in Fig. 3a. The dashed curve represents the initial spectrum reduced in amplitude by 4 times; the shaded area corresponds to the range of long-wavelength IR radiation (5–10 μm).

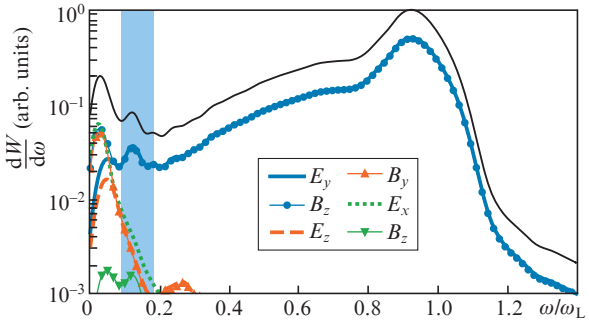

Figure 4. (Colour online) Component-wise energy spectrum of the electromagnetic field for the distance specified by the vertical dashed line in Fig. 3a. The thin black solid curve is the total spectrum coinciding with the instantaneous spectrum in Fig. 3b; the shaded area corresponds to the wavelength range of 5–10 μm.

The component-wise analysis (Fig. 4) also allows us to evaluate the reliability of the approximation concerning the fulfilment of the vacuum dispersion relation. In the numerical simulation performed, we did not derive the spatial density distribution of the currents, which did not allow us to directly estimate their spectral amplitude for various wave vectors. However, it is clear that their spectral components are concentrated in the same region as the fields of the wake wave and electron bunch they generate, i.e., mainly in the wavelength region above 10 μm. The equality of contributions of components E_y and B_z with almost complete absence of contributions of other components is also an indirect evidence of the fulfilment of the vacuum dispersion relation for wavelengths shorter than 10 μm, which is expected for an electromagnetic wave in vacuum. Thus, in the wavelength range of 5–10 μm, the spectrum calculation using the vacuum dispersion relation is correct.

Figure 5 shows the dependence of the fraction of the initial pulse energy in IR radiation as a function of the distance travelled by the laser pulse. By the end of the simulation, about 53% of the initial laser pulse energy remains in the electromagnetic field (both in the laser field and IR field); the remaining energy is absorbed by the plasma and spent on the wake wave excitation. Herewith, about 1% of the laser energy (i.e. ~0.1 J) is transferred to the field corresponding to the long-wavelength IR range (5–10 μm), which coincides in order of magnitude with the results obtained in works [1, 2, 5].

Figure 6 shows the distribution of the transverse electric field E_y and the instantaneous power $P = \int S_x \mathrm{d}^2\boldsymbol{r}_\perp$ (where $\boldsymbol{S}$ is the Poynting vector) as a function of the longitudinal coordinate for spectral components in the range 5–10 μm for two different time moments shortly before and after leaving the gas jet. In this case, IR radiation is present both in the front and back parts of the plasma cavity, and also penetrates into the second cavity located outside the simulation region, which is consistent with the results of previous studies (see, for example, work [4]). The study of IR radiation penetration in

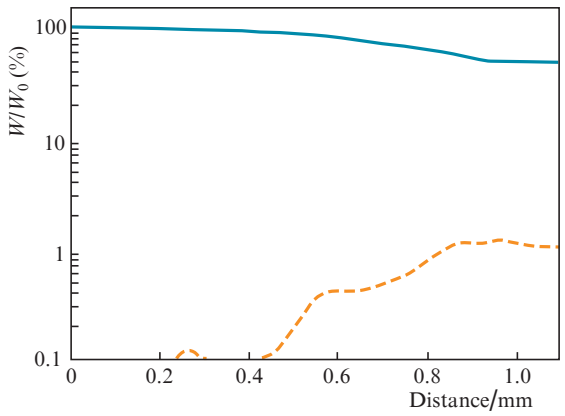

Figure 5. (Colour online) Energy fraction in the laser field (wavelengths shorter than 5 μm, solid curve) and in long-wavelength IR radiation (wavelengths from 5 to 10 μm, dashed curve) as a function of the distance travelled by the laser pulse with respect to the initial laser pulse energy W_0.

subsequent periods of wake wave oscillations requires calculations with a longer simulation domain and a better resolution, since the contribution of simulation errors increases when moving in the opposite direction along the wake wave. In addition, the ingenious effect is that the central part of the plasma cavity does not virtually contain IR radiation, which in the range of 5–10 μm is represented in the form of two consecutive pulses with a duration of about 40 fs (FWHM). The explanation of this effect requires additional investigation. To simulate the further propagation of the IR pulse, it is necessary to increase the simulation domain in the transverse direction, since the pulse focused in plasma to a size of several tens of micrometres begins to rapidly diffract and reaches the simulation domain boundaries.

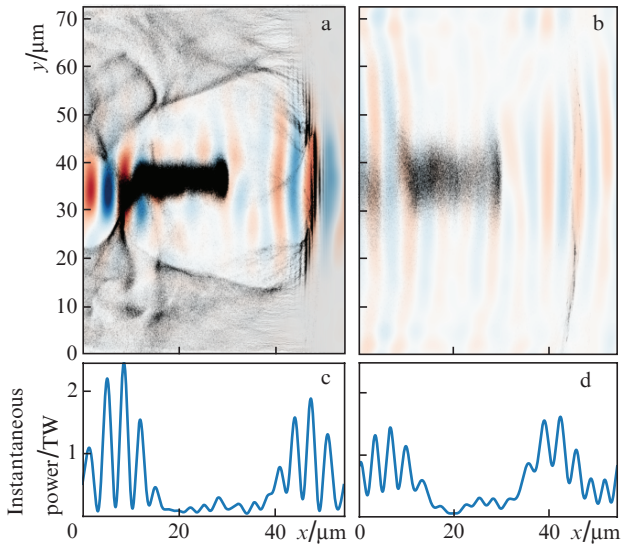

Figure 6. (Colour online) Distribution of the transverse electric field E_y for the spectral components in the wavelength range of 5–10 μm in the wake wave in the cross section by the xy plane (a, b) and the instantaneous power of these spectral components (c, d) after the passage by the laser pulse in plasma the distances of (a, c) 0.86 and (b, d) 1.09 mm. The electron density distribution is shown in black.

4. Conclusions

The paper demonstrates the possibility of using laser pulses shortened using CafCA to generate long-wavelength IR radiation when interacting with a gas jet, which can be implemented on the PEARL laser facility. As in works [4, 5], the use of ultrashort pulses is important for more efficient generation of IR radiation. In particular, a similar simulation conducted for a pulse with the same energy and waist size, but with a duration of 60 instead of 20 fs, has shown that by the end of the simulation, the efficiency of generating long-wave IR radiation does not exceed 0.1%.

In comparison with works [4, 5] in which the temporal pulse compression was performed using a rather complex longitudinal profile of the plasma target, the use of a gas jet simplifies the experiment and allows us to modify the target parameters completely independently of the laser pulse parameters. However, in this case, in contrast to works [4, 5], in which the generation of ultrashort (virtually single-period) IR pulses was observed, two pulses with a duration of about 40 fs have been generated.

Acknowledgements. This work was supported by the Russian Science Foundation (Grant No. 18-11-00210, I.Yu.K., simulation of laser-plasma interaction) and the Russian Foundation for Basic Research (Grant No. 20-02-00691, A.A.G., spectral analysis).

References

1. Pai C.-H., Chang Y.-Y., Ha L.-C., Xie Z.-H., Lin M.-W., Lin J.-M., Chen Y.-M., Tsaur G., Chu H.-H., Chen S.-H., Lin J.-Y., Wang J., Chen S.-Y. *Phys. Rev. A*, **82**, 063804 (2010).
2. Zhu W., Palastro J.P., Antonsen T.M. *Phys. Plasmas*, **20**, 073103 (2013).
3. Wilks S.C., Dawson J.M., Mori W.B., Katsouleas T., Jones M.E. *Phys. Rev. Lett.*, **62**, 2600 (1989).
4. Nie Z., Pai C.-H., Zhang J., Ning X., Hua J., He Y., Wu Y., Su Q., Liu S., Ma Y., et al. *Nat. Commun.*, **11**, 2787 (2020).
5. Nie Z., Pai C.-H., Hua J., Zhang C., Wu Y., Wan Y., Li F., Zhang J., Cheng Z., Su Q., et al. *Nat. Photonics*, **12**, 489 (2018).
6. Strickland D., Mourou G. *Opt. Commun.*, **55**, 447 (1985).
7. Khazanov E.A., Mironov S.Yu., Mourou G. *Phys. Usp.*, **62** (11), 1096 (2019) [*Usp. Fiz. Nauk*, **189** (11), 1173 (2019)].
8. Danson C.N., Haefner C., Bromage J., Butcher T., Chanteloup J.-C.F., Chowdhury E.A., Galvanauskas A., Gizzi L.A., Hein J., Hillier D.I., et al. *High Power Laser Sci. Eng.*, **7**, e54 (2019).
9. Lozhkarev V.V., Freidman G.I., Ginzburg V.N., Katin E.V., Khazanov E.A., Kirsanov A.V., Luchinin G.A., Mal'shakov A.N., Martyanov M.A., Palashov O.V., Poteomkin A.K., Sergeev A.M., Shaykin A.A., Yakovlev I.V. *Laser Phys. Lett.*, **4**, 421 (2007).
10. Ginzburg V.N., Yakovlev I.V., Zuev A.S., Korobeynikova A.P., Kochetkov A.A., Kuzmin A.A., Mironov S.Yu., Shaykin A.A., Shaikin I.A., Khazanov E.A. *Quantum Electron.*, **49** (4), 299 (2019) [*Kvantovaya Elektron.*, **49** (4), 299 (2019)].
11. Mironov S.Yu., Starodubtsev M.V., Khazanov E.A. *Opt. Lett.*, **46**, 1620 (2021).
12. Birdsall C.K., Langdon A.B. *Plasma physics via computer simulation* (CRC press, 2004).
13. Pukhov A. *CERN Yellow Rep.*, **1**, 181 (2016).
14. Quill, https://github.com/QUILL-PIC/Quill.
15. Pukhov A. *J. Plasma Phys.*, **61**, 425 (1999).
16. Mangles S.P.D., Genoud G., Bloom M.S., Burza M., Najmudin Z., Persson A., Svensson K., Thomas A.G.R., Wahlström C.-G. *Phys. Rev. ST Accel. Beams*, **15**, 011302 (2012).
17. Lu W., Tzoufras M., Joshi C., Tsung F.S., Mori W.B., Vieira J., Fonseca R.A., Silva L.O. *Phys. Rev. Sel. Top. Accel. Beams*, **10**, 061301 (2007).